Supporting Information

Fabrication of cuprous nanoparticles in MIL-101: An efficient adsorbent for the separation of olefin/paraffin mixtures

Ganggang Chang[†], Zongbi Bao*[†], Qilong Ren[†], Shuguang Deng[†‡], Zhiguo Zhang[†], Baogen Su[†], Huabin Xing[†], and Yiwen Yang[†]

[†]*Key Laboratory of Biomass Chemical Engineering of the Ministry of Education, Department of Chemical and Biological Engineering, Zhejiang University, Hangzhou 310027, China*

[‡]*Chemical Engineering Department, New Mexico State University, Las Cruces, NM 88003, USA*

Email: baozb@zju.edu.cn

RSC Adv.

I. Synthesis of MIL-101

MIL-101 was synthesized and purified according to the reported method.[1] Briefly, 8.0 g $Cr(NO_3)_3$ (0.02 mol), 3.28 g terephthalic acid (TPA) (0.02mol), 300 μL aqueous HF solution (37wt%) and 140 mL ultrapure water were transformed into a 250 mL Teflon-lined stainless steel autoclave and sealed, and then heated up to 220 ^oC for 8h. After that, the autoclave was slowly cooled down to ambient temperature. The green suspension of MIL-101 was filtered by using a stainless steel meshwork (diameter of 61 μm) to remove the recrystallized needle-shaped colorless TPA, which retained on the meshwork, and the MIL-101 suspension passed through the meshwork. The filtrated MIL-101 suspension was subsequently centrifuged at 3500×g (for 10 min to collect the first precipitates of MIL-101) and 8000×g (for 20 min to collect the second precipitates of MIL-101), respectively. The second precipitates of MIL-101 were washed several times with ultrapure water, and dried at 100 ^oC for 24 h in an air oven.

II. Preparation of Cu^+@MIL-101

To prevent metal nanoparticles (MNPs) aggregation on external surfaces of MIL-101 framework, we used the "double solvents" method,[2] which is based on a hydrophilic solvent (concentrated hydrochloric acid solution) and a hydrophobic solvent (hexane), the former containing the metal precursor with a volume set equal to or less than the pore volume of the adsorbent (i.e. MIL-101), which can be absorbed within the hydrophilic adsorbent pores and the latter, in a large amount, playing an important role to suspend the adsorbent and facilitate the impregnation process. Since the inner surface area of MIL-101 is much larger than the outer surface area, the small amount of aqueous MNP (equal or less than pore volume) could go inside the hydrophilic pores by capillary force, which greatly minimizes the deposition of MNP on the outer surface. Typically, for loading Cu^+ inside the cavities of MIL-101, 100 mg of green MIL-101 powder activated by heating at 150 °C for 12 h under dynamic vacuum, which has a pore volume of 2.12 $cm^3\ g^{-1}$ as determined by N_2 sorption isotherm, was suspended in dry n-hexane (20 mL), to which an aqueous HCl solution (0.20 mL) with different CuCl concentrations was added dropwise under continuous vigorous stirring during 15 minutes. After careful filtration, the green powder was dried under high vacuum at the temperature of 50 ^oC.

III. Characterization of MIL-101 and Cu^{+}@MIL-101

Adsorption isotherms of N_2 on these adsorbents were obtained at 77 K by an Autosorb-1MP-VP apparatus (Quantachrome Corp., USA). Adsorbents were evacuated overnight at 180 °C to remove the water molecules prior to the nitrogen adsorption experiments. Specific surface areas of adsorbents were calculated by the Brunauer-Emmett-Teller (BET) method over a pressure range of $0.05 < p/p_0 < 0.30$ and the total pore volume was determined from the amount adsorbed at a relative pressure of about 0.98 using adsorption data of nitrogen adsorption isotherm.

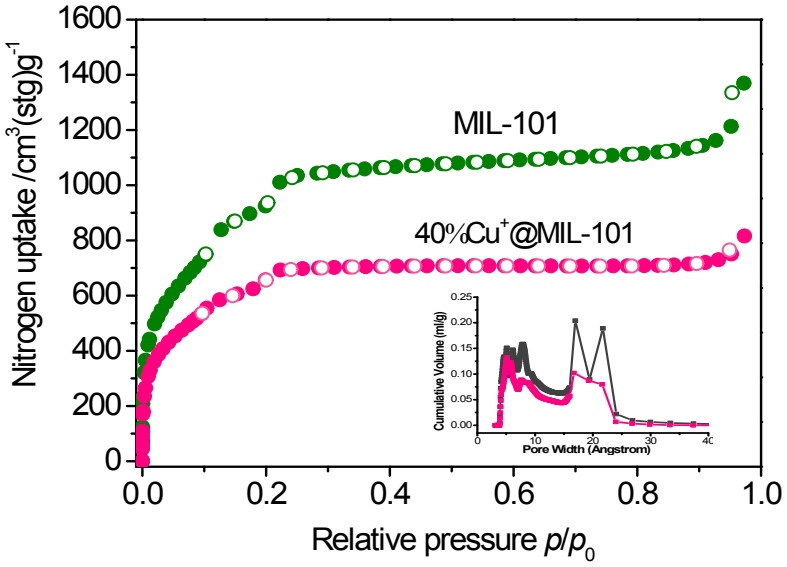

Figure S1. Isotherms of N_2 on the MIL-101 and Cu^{+}@MIL-101at 77K. (The inset is the pore size distribution curve).

Powder X-ray diffraction (XRD) patterns of MIL-101 and Cu^{+}@MIL-101 were recorded on a XPert diffractometer (Panalytical Corp., Netherlands) which was operated at 40 kV for CuKa (λ= 0.1543 nm) radiation from 3° to 80° (2θ angle range) with a scan step size of 0.02°. Scanning electron microscope (SEM) was performed on a SIRION-100 instrument. Scanning was performed on a sample powder previously dried and sputter-coated with a thin layer of gold. Transmission electron microscope (TEM) images were taken at 80 kV by a JEM-1230 (JEOL Corp., Japan). XPS measurements were performed on a combined VG ESCALAB MARK II instrument at a base pressure of 7.1×10^{-10} mbar which was operated at Mg *K*α: 1253.6eV, CAE: 50eV and Step: 0.2eV, 0.5eV. The thermal stability of MIL-101 was investigated by thermal

gravimetric analysis (TGA) with SDT Q600 (AT Corp., USA) from 40 °C to 800 °C with a ramping rate of 2.0 °C/min in the air atmosphere. Fourier transform infrared (FT-IR) spectrum was determined using Bruker-vector-22 (German) with a range of 500-4000 cm^{-1}. MIL-101 sample for FT-IR analysis was pretreated by grinding power of MIL-101 together with KBr in an agate mortar and then pressing them into flakes by a tablet machine.

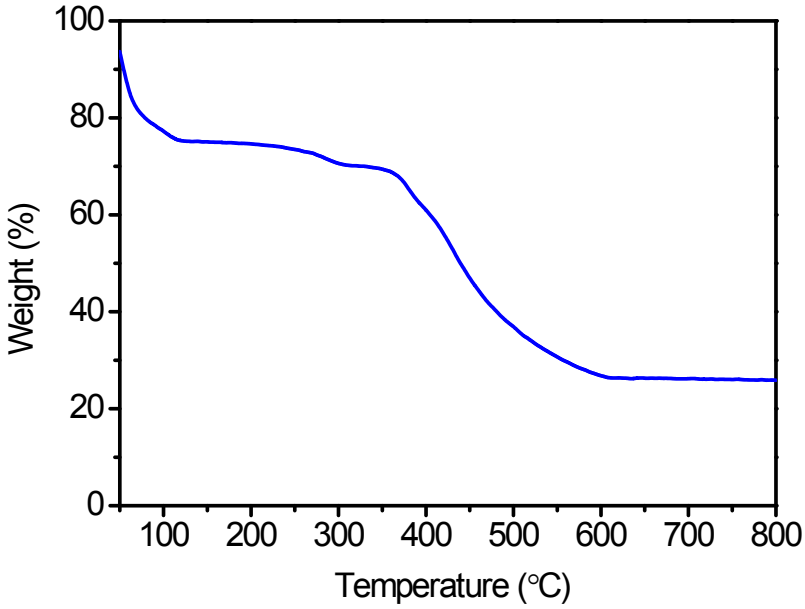

Figure S2. TGA curve of MIL-101. The TGA profile shows that MIL-101 is stable up to 270 °C. A total of 75% weight loss of MIL-101, mainly occurred between 270 and 550 °C, may result from the framework decomposition of the organic moieties.

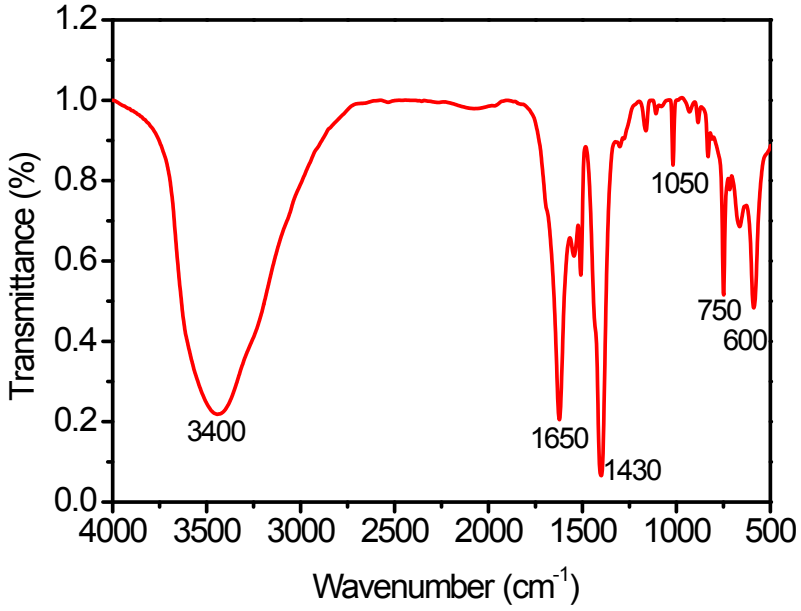

Figure S3. FT-IR spectrum of MIL-101. The FT-IR spectrum of MIL-101 is similar to the previous result.[3] The strong bands, at 1650 and 1430 cm^{-1}, can be ascribed to the vibrational stretching frequencies of the framework (O-C-O). The bands at 1055 and 750 cm^{-1}can be assigned to the vibrations of benzene rings. The bands near 600 cm^{-1} are most likely to ascribe to in-plane and out-of-plane bending modes of COO-groups.

IV. Gas sorption measurements

Adsorption equilibrium and diffusivity data of ethane and ethylene were measured volumetrically in a Micromeritics ASAP 2050 adsorption apparatus. The adsorption isotherms were obtained at three temperatures (303, 313, and 323 K) and gas pressures up to 1 bar. The temperatures were controlled by using a Dewar with a circulating jacket connected to a thermostatic bath with a precision of ±0.01 ^{o}C. About 100 mg of adsorbent sample was used for the gas adsorption studies. The initial outgassing process was carried out under a vacuum at 180 ^{o}C for 12 h. The free space of the system was determined by using the helium gas. The degas procedure was repeated on the same sample between measurements for 2 h. Ultrahigh purity grade helium (99.999%), ethane (99.99%), and ethylene (99.99%) were purchased from Jingong Co., Ltd. (China). All hydrocarbons were used as received without any purification.

The adsorption kinetic uptake curves (adsorption amount as a function of time) were obtained at the same time when the adsorption equilibrium data were collected. After the adsorbate gas was introduced into the adsorption system at a given dose, the changes in gas pressure and adsorption volume with time were recorded and then converted into the transient adsorption amount as a function of time. The transient adsorption uptakes generated the adsorption kinetics, and the final adsorption amount at the terminal pressure determined the adsorption equilibrium amount at a given pressure. In all experiments, the uptake curves were measured at a stepped pressure increment from 60 to 70 mmHg.

All the adsorption isotherms are reversible, which was confirmed by measuring the desorption braches and all the adsorption isotherms could be described very well by Double-site Langmuir model [4]as shown in Eq. 1.

$$q = q_c \frac{K_c P}{\left(1 + K_c P\right)} + q_i \frac{K_i P}{\left(1 + K_i P\right)} \tag{1}$$

where the subscript *c* and *i* represent the channels and intersections, respectively. The geometrical constraint gives rise to two different saturation amounts adsorbed in locations *c* and *i*, and indicated by q_c and q_i. This description of adsorption equilibrium contains four parameters and their values are obtained from the experimental data by nonlinear regression.

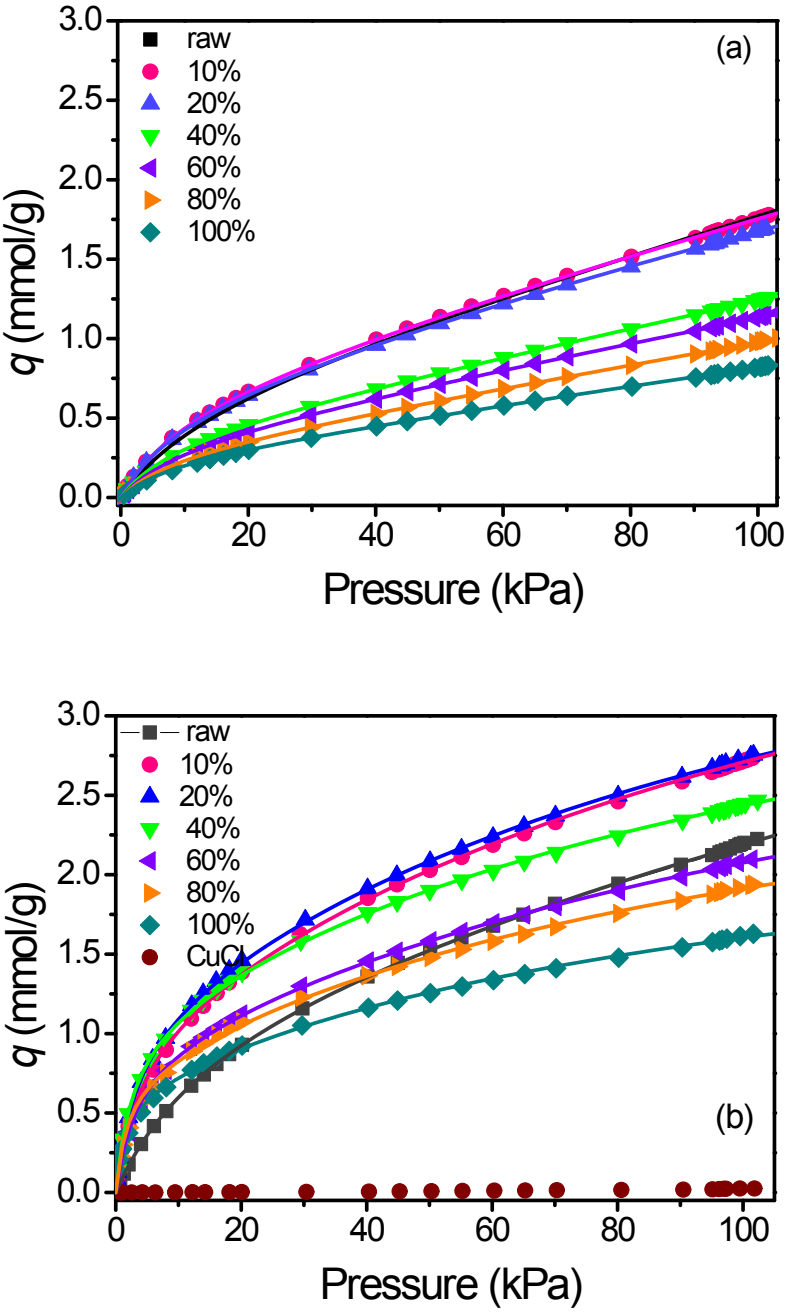

Figure S4. Adsorption isotherms of ethane (a) and ethylene (b) on the parent and Cu^{+}@MIL-101 that with varied Cu^{+} loadings at 30 °C and 1bar. The lines are fitted results by double-site Langmuir model

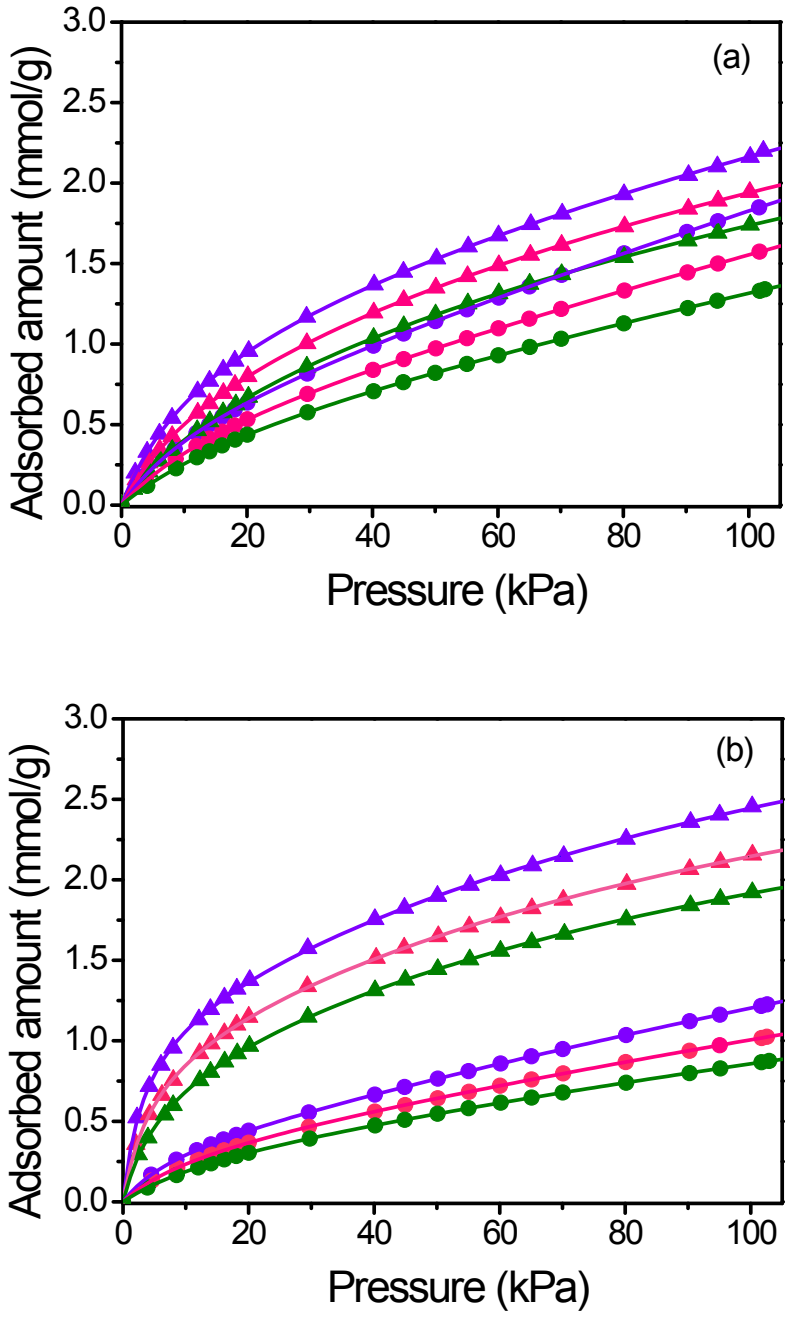

Figure S5 Adsorption isotherms of ethane (●) and ethylene (▲) on the parent (a) and 40%Cu^{+}@MIL-101(b) at 1 bar and at temperature of 30 °C (blue), 40 °C (red) and 50 °C (green). The lines are fitted results by double-site Langmuir model

V. Henry constants and equilibrium selectivity

The values of Henry constants are an alternative way to understand the interaction between adsorbate and adsorbent. An extrapolation method was used to determine the Henry constants, which is based on the isotherm model in Virail form. The adsorption isotherm can be expressed by

$$P = \frac{q}{H}\exp(A_1 q + A_2 q^2 + ...) \qquad (2)$$

where A_1 and A_2 are Virial coefficients and H is the Henry constant. According to Eq. 2, the plot of ln(P/q) vs q is a linear function of when q or P approaches zero. The following equation was obtained for the linear region:

$$\ln(\frac{P}{q}) = A_1 q - \ln H \qquad (3)$$

The Henry constant can be extracted by extrapolating the intercept of Eq 3. In order to evaluate the efficacy of an adsorbent for gas separation and purification of by adsorption, it is necessary to know the adsorbent properties including adsorption capacity and selectivity. The adsorption equilibrium selectivity between components 1 and 2 is defined as

$$\alpha_{12} = \frac{H_1}{H_2} \qquad (4)$$

where component 1 is the stronger adsorbate and 2 is the weaker adsorabte. The equilibrium selectivity defined in the above equation is basically the ratio of the Henry's constants of the two components, which is the intrinsic selectivity that is only valid at very low gas pressure and low adsorption loading on the adsorbent.

VI. Adsorbent selection parameter *S*

For pressure swing adsorption process, the adsorbent selection parameter S defined in the following equation is more useful in adsorbent evaluation and selection because it includes the ratio of adsorption capacity difference of components 1 and 2: [5]

$$s=\frac{\Delta q_1}{\Delta q_2}\alpha_{12} \qquad (5)$$

where Δq_1 and Δq_2 are the working capacity that is calculated as the adsorption equilibrium capacity difference at adsorption pressure and desorption pressure for components 1 and 2, respectively

Ideal Adsorbed Solution Theory (IAST) [6] was applied to the modeled isotherms to determine the selectivity for ethylene and ethane, the selectivity on different adsorbents is calculated via Eq.6

$$s_{ij}=\frac{x_i / x_j}{y_i / y_j} \qquad (6)$$

where x_i and x_j are the equilibrated adsorption capacity of ethylene and ethane respectively, and y_i and y_j are the molar fractions of ethylene and ethane in gas phased respectively.

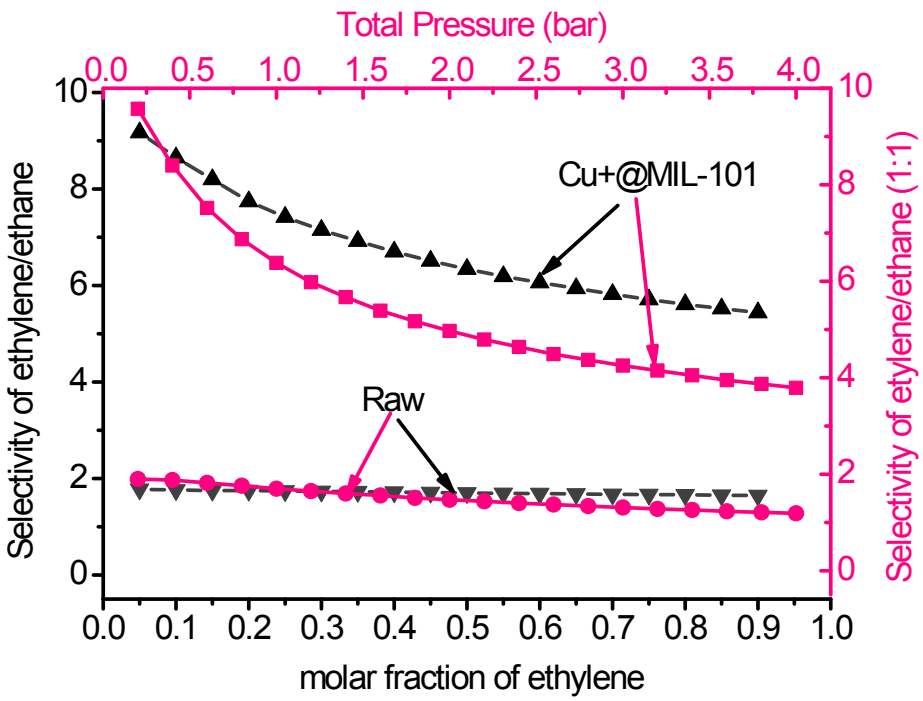

Figure S6. Selectivity of C_2H_4 over C_2H_6 on the parent and 40%Cu^+@MIL-101 with different molar fraction and varied total pressure at 30 °C.

VII. Heat of adsorption

The isosteric heat of adsorption represents the strength of the interactions between adsorbate molecules and the adsorbent lattice atoms and can provide useful information about the energetic heterogeneity of a solid surface. It is also an important aspect when adsorbents are evaluated for potential adsorption processes. The isosteric heat of adsorption (Q_{st}) at a given amount can be calculated by the Clausius-Clapeyron equation as:

$$Q_{st} = -RT^2 \left(\frac{\partial \ln p}{\partial T}\right)_{n_a} \qquad (7)$$

where Q_{st}(kJ mol^{-1}) is the isosteric heat of adsorption, p is the pressure (kPa), T is the temperature, R is the gas constant, and n_a is the adsorption amount (mmol/g). Integration of Eq. 7 gives

$$\ln p = \frac{Q_{st}}{RT} + C \qquad (8)$$

The heat of adsorption at a given uptake was calculated from the slopes of the isosteres according to Eq. 8.

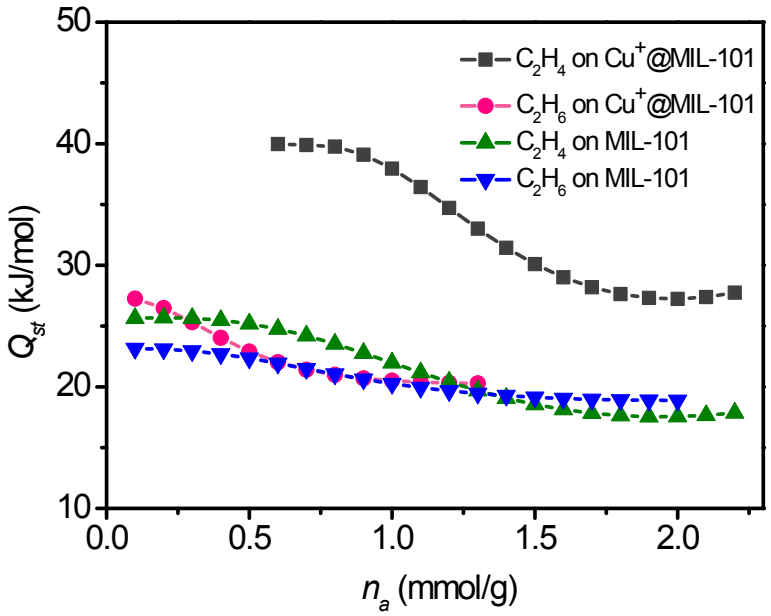

Figure S7. Isosteric heat of adsorption as a function of loading for ethylene and ethane on the parent and Cu^+@MIL-101

VIII. Adsorption Kinetics

To extract the intracrystalline diffusivity, a simplified micropore diffusion model was used. Assuming mass transfer resistance in micropores is more important and the adsorbent crystals can be regarded as an approximately spherical object, the adsorption uptake profiles can be described by the following equation [7]

$$\frac{\bar{q}-q_0'}{q_0-q_0'}=\frac{m_t}{m_\infty}=1-\frac{6}{\pi^2}\sum_{n=1}^{\infty}\frac{1}{n^2}\exp\left(-\frac{n^2\pi^2 D_c t}{r_c^2}\right) \qquad (9)$$

where $\bar{q}$ is the average adsorption amount in the particle, q_0' is the initial adsorption amount in the particle, q_0 is the equilibrium uptake in the particle, and m_t/m_∞ is the fractional adsorption uptake. At short times, Eq. 9 is approximated by

$$\frac{m_t}{m_\infty}=\frac{6}{\sqrt{\pi}}\sqrt{\frac{D_c}{r_c^2}t}-3\frac{D_c}{r_c^2}t \qquad (10)$$

This expression is accurate to within 1% for m_t/m_∞ <0.85 (or $D_c t/r_c^2$ < 0.4). In this study, the diffusion time constant $D_c t/r_c^2$ was used as fitting parameters to correlate Eq. 9 to the experimental data.

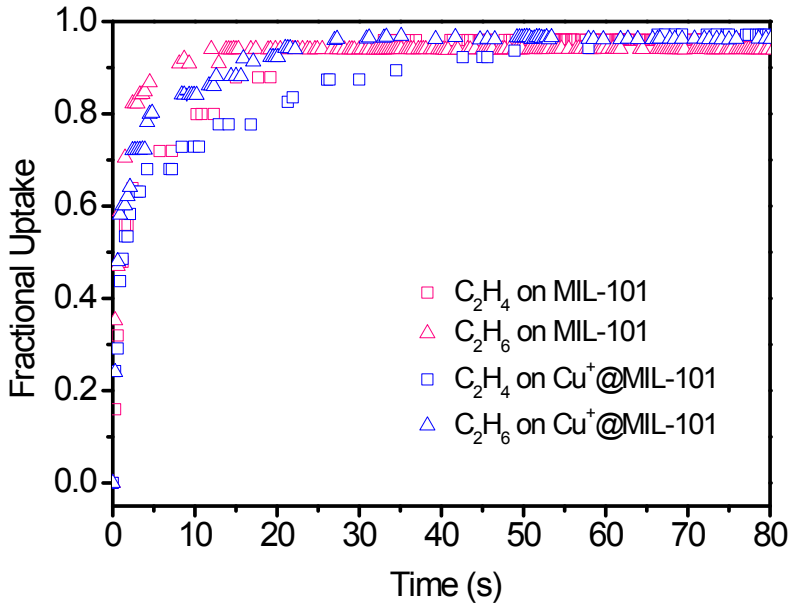

Figure S8. Adsorption kinetics of ethylene and ethane on the parent and 40%-Cu^+@MIL-101 at 30 °C and at a pressure of 60 mmHg.

IX. Packed Bed Adsorber Breakthrough Simulations

For a rational choice of adsorbents for mixture separation we need to have a proper method of evaluation that combines the selectivity and capacity metrics in a manner that is a true reflection of the separation performance of a PSA unit. For this purpose we perform transient breakthrough calculations to compare the adsorptive separation between raw MIL-101 and Cu^{+}-loaded MIL-101, using Aspen^{TM} Adsorption software program.

Assuming plug flow of the gas mixture through the fixed bed maintained under isothermal conditions and negligible pressure drop without both axial and radial dispersion, the partial pressure of component *i* in the gas phase at any position and instant of time is calculated using the following general material balance equation:

$$\frac{1}{RT}\varepsilon\frac{\partial p_i}{\partial t} = -\frac{1}{RT}\frac{\partial\left(up_i\right)}{\partial z} - \left(1-\varepsilon\right)\rho\frac{\partial q_i}{\partial t};\ i = 1,2 \qquad (11)$$

In equation (11), t is the time, z is the distance along the adsorber, ρ is the framework density, ε is the bed voidage, u is the superficial gas velocity, and q_i is the transient loading of species i on the adsorbent.

The mass transfer from the gas to the solid phase is expressed by a linear driving force (LDF) model:

$$\rho\frac{\partial q_i}{\partial t} = k_{MTC_{s,i}}\left(q_i^{*} - q_i\right) \qquad (12)$$

With q_i* being the loading which is in equilibrium with the gas phase composition. The main resistances to mass transfer are combined in a lumped parameter k_{MTC}.

The boundary conditions for fluid flow are given as:

$$t \geq 0;\ p_i\left(t,0\right) = p_i^0 = p_t x_i^0 \qquad (13)$$

and the adsorber bed is initially free of adsorbates, thus the initial condition can be written as:

$$t = 0;\ q_i\left(0, z\right) = 0 \qquad (14)$$

The molar loading of the species *i*, q_i, at any position z, and time *t* is determined from IAST. Equation (11) is first subjected to finite volume discretization by upwind differencing scheme (UDS) in conjunction with the Gear integration. Typically, the adsorber length *L* is divided into a uniform grid of 20 slices. Specifically, the calculations were performed taking the following parameter values: L = 0.15 m; ε = 0.4; u = 0.18 cm/s (at inlet). The feed mixture to the adsorber is ternary ethane/ethylene/helium gas mixture maintained at isothermal conditions at 303 K. The helium is used as carrier gas. In these calculations the molar fraction of ethane and ethylene are taken to be equal to each other, i.e. $x_1 = x_2 = 0.005$, thus the total pressure of feed fluid initially set at 100 bar can be regarded as constant as well as the isothermal behavior of the fixed bed even when ethane and ethylene are adsorbed by the sorbent. The total mass of the adsorbents used is governed by the framework density ρ. The values of the framework densities used in the breakthrough simulations are 300 kg/m^3 and 420 kg/m^3 for raw MIL-101 and Cu^+@MIL-101, respectively. The effective mass-transfer coefficients of k_{MTC} were taken as $15D_c/r^2$ as shown in Table S4.

Table S1. Summary of surface area of adsorbents (S_{BET}), Henry's constants (H), equilibrium selectivity (α) and adsorbent selection parameter (S) calculated from the single-component adsorption isotherms

Cu^+@ MIL-101	S_{BET} (m^2/g)	V_p (cm^3/g)	q (mmol/g)		H(mmol/g/kPa)		α_{ij}	S_{ij}
			C_2H_4	C_2H_6	C_2H_4	C_2H_6		
Raw	3120	2.12	2.22	1.84	0.0935	0.0583	1.60	1.9
10%	2228	1.52	2.73	1.77	0.3734	0.0726	5.14	6.6
20%	1813	1.23	2.75	1.68	0.5071	0.07037	7.21	10.0
40%	1587	1.01	2.46	1.22	0.7034	0.0501	14.0	20.9
60%	1299	0.85	2.10	1.11	0.4059	0.0420	9.66	14.6
80%	1130	0.78	1.94	0.98	0.5559	0.0365	15.2	21.3
100%	877	0.55	1.64	0.83	0.5642	0.0342	16.5	23.9

Table S2. Comparison of equilibrium adsorption amount of ethylene/ethane and their ratio between MIL-101 and other adsorbents at about 303 K and 1 bar

Adsorbent	*q* (mmol/g)		$q(C_2H_4)/q(C_2H_6)$	ref.
	C_2H_4	C_2H_6		
Activated carbon (303K)	1.8	2.6	0.69	8
Ag-ETS (298K)	1.12	1.01	1.11	9
CMK-3 (303k)	2.8	3	0.93	10
Cu-CMK-3 (303K)	3.15	1.25	2.52	10
HMS (303K)	0.4	0.6	0.67	11
UTSA-33 (273K)	2.6	2.4	1.08	12
HKUST-1 (295K)	—	—	<2	13
Mg-MOF-74 (298K)	6.8	7	0.97	14
Co-MOF-74(293K)	4.5	4	1.125	15
Fe-MOF-74 (318K)	—	—	1.28	16
ZIF-7 (298K)	1.75	1.75	1	17
ZIF-8 (293K)	1.5	2.5	0.60	15
MIL-101 (303K)	2.22	1.84	1.21	this work
MIL-101@Cu^+ (303K)	2.46	1.22	2.02	this work

Table S3. Summary of equation parameters of the double-site Langmuir model for the adsorption of ethylene and ethane on the parent and 40%Cu^+@MIL-101

sample	T(°C)	adsorbate	q_c (mmol/g)	K_c (kPa^{-1})	q_i (mmol/g)	K_i (kPa^{-1})	r^2
MIL-101	30	C_2H_4	1.07321	0.08148	6.56171	0.00225	0.9999
		C_2H_6	0.66245	0.06764	75.5458	0.00017	0.9999
	40	C_2H_4	0.87347	0.06609	4.60923	0.00344	0.9999
		C_2H_6	0.60999	0.05454	43.30703	0.00025	0.9999
	50	C_2H_4	0.74308	0.05311	4.15712	0.00365	0.9999
		C_2H_6	0.56813	0.04169	21.75872	0.00041	0.9999
40% Cu^+@MIL-101	30	C_2H_4	1.13347	0.30316	3.48271	0.00631	0.9998
		C_2H_6	0.36096	0.11893	10.39524	0.00091	0.9999
	40	C_2H_4	0.93479	0.22836	3.03886	0.00699	0.9998
		C_2H_6	0.34759	0.08409	9.10131	0.00083	0.9999
	50	C_2H_4	0.77425	0.17705	2.82702	0.00719	0.9999
		C_2H_6	0.32907	0.06205	8.21283	0.00075	0.9999

Table S4. Comparison of diffusion time constants of ethylene and ethane in MIL-101 and other adsorbents at about 30 °C

Adsorbent	Adsorbate	$D_c/r_c^2(s^{-1})$	ref.
MIL-101	ethylene	2.86×10^{-2}	this work
MIL-101	ethane	5.72×10^{-2}	this work
Cu+@MIL-101	ethylene	2.06×10^{-2}	this work
Cu+@MIL-101	ethane	3.79×10^{-2}	this work
Mg-MOF-74	ethylene	7.12×10^{-3}	14
Mg-MOF-74	ethane	1.39×10^{-3}	14
Zeolite 4A	ethylene	5.12×10^{-3}	18
Zeolite 4A	ethane	1.64×10^{-4}	18
Ag^+-resin	ethylene	1.03×10^{-4}	19
Ag^+-resin	ethane	8.7×10^{-4}	19

Reference

1. a) G. Ferey, C. Mellot-Draznieks, C. Serre, F. Millange, J. Dutour, S. Surble and I. Margiolaki, *Science*, 2005, 309, 2040-2042; b) K. Yang, Q. Sun, F. Xue and D. Lin, *J. Hazard. Mater.*, 2011, **195**, 124-131.
2. A. Aijaz, A. Karkamkar, Y. J. Choi, N. Tsumori, E. Rönnebro, T. Autrey, H. Shioyama and Q. Xu, *J. Am. Chem. Soc.*, 2012, **134**, 13926-13929.
3. Z. Y. Gu and X. P. Yan, *Angew. Chem. Int. Ed.*, 2010, **49**, 1477-1481.
4. W. Zhu, J. M. Van de Graaf, L. J. P. Van den Broeke, F. Kapteijn and J. A. Moulijn, *Ind. Eng. Chem. Res.*, 1998, **37**, 1934-1942.
5. a) R. T. Yang, *Adsorbents : Fundamentals and Applications*, Willey-Interscience : New York, 2003; b) D. Saha, Z. Bao, F. Jia and S. Deng, *Environ. Sci. Technol.*, 2010, **44**, 1820-1826.
6. Z. J. zhang, Z. Li and J. Li, Langmuir, 2012, **28**, 12122-12138.
7. D. M. Ruthven, S. Farooq and K.S. Knaebel, Pressure Swing Adsorption; VCH Publishers New York, 1994.
8. B.-U. Choi, D.-K. Choi, Y.-W. Lee and B.-K. Lee, *J. Chem. Eng. Data*, 2003, **48**, 603-607.
9. A. Anson, Y. Wang, C. C. H. Lin, T. M. Kuznicki and S. M. Kuznicki, *Chem. Eng. Sci.*, 2008, **63**, 4171-4175.
10. W.-J. Jiang, L.-B. Sun, Y. Yin, X.-L. Song and X.-Q. Liu, *Sep. Sci.Technol.*, 2013, **48**, 968-976.
11. B. L. Newalkar, N. V. Choudary, U. T. Turaga, R. P. Vijayalakshmi, P. Kumar, S. Komarneni and T. S. G. Bhat, *Micropor. Mesopor. Mater.*, 2003, **65**, 267-276.
12. Y. He, Z. Zhang, S. Xiang, F. R. Fronczek, R. Krishna and B. Chen, *Chem. Eur. J.*, 2012, **18**, 613-619.
13. S. Wang, Q. Yang and C. Zhong, *Sep. Purif. Technol.*, 2008, **60**, 30-35.
14. Z. Bao, S. Alnemrat, L. Yu, I. Vasiliev, Q. Ren, X. Lu and S. Deng, *Langmuir*, 2011, **27**, 13554-13562.
15. U. Böhme, B. Barth, C. Paula, A. Kuhnt, W. Schwieger, A. Mundstock, J. Caro and M. Hartmann, *Langmuir*, 2013, **29**, 8592-8600.
16. E. D. Bloch, W. L. Queen, R. Krishna, J. M. Zadrozny, C. M. Brown and J. R. Long, *Science*, 2012, **335**, 1606-1610.
17. C. Gucuyener, v. d. Bergh, J. Gascon and F. Kapteijn, *J. Am. Chem. Soc.*, 2010, **132**, 17704-17706.
18. S. U. Rege, J. Padin and R. T. Yang, *AIChE J.*, 1998, **44**, 799-809.
19. Z. B. Wu, S. S. Han, S. H. Cho, J. N. Kim, K. T. Chue and R. T. Yang, *Ind. Eng. Chem. Res.*, 1997, **36**, 2749-2756.